

Seasonal Variability of Eddy Kinetic Energy in the Central Indian Ocean: POLYGON-67 Revised

G. I. Shapiro ✉, J. M. Gonzalez-Ondina

University of Plymouth, Plymouth, United Kingdom

✉ gshapiro@plymouth.ac.uk

Purpose. The main goal of this study is to analyse the seasonal variability of meso-scale eddy activity in the north tropical Indian Ocean. The selected area coincides with the location of POLYGON-67 (P67) experiment where the mesoscale eddies of the open ocean were first discovered.

Methods and results. The variability of mesoscale eddy kinetic energy in surface ocean layer, enstrophy of larger scale circulation, spatial and temporal patterns of surface currents and surface winds are jointly analysed using a 20-year long daily time series of eddy-resolving ocean reanalysis data obtained from EU Copernicus Marine Environment Monitoring Service and climatic wind data from US National Oceanographic and Atmospheric Administration. The fast mesoscale and slow large-scale processes are separated using a Savitsky – Golay filter with the cut-off time of 103 days which corresponds to a local minimum in the full kinetic energy power spectrum. In contrast to other parts of the tropical ocean, the seasonal variability of *EKE* exhibits 2 maxima – the largest being in April, and the secondary being in October which are related to the maxima in enstrophy of larger scale currents.

Conclusions. The double peak variability in *EKE* corresponds to the seasonal variability of large scale enstrophy and monsoon wind circulation and supports a hypothesis that the main mechanism of *EKE* generation is barotropic instability of larger scale currents. The *EKE* variability within P67 is mostly controlled by advection of energy from neighbouring areas, and to a lesser extent by local generation.

Keywords: ocean circulation, mesoscale eddies, seasonal variability, reanalysis, barotropic instability, Indian Ocean

Acknowledgements: the authors are grateful to Mrs S.B.Sharpe for proofreading the manuscript. This study was partially supported by the University of Plymouth and University of Plymouth Enterprise LTD.

For citation: Shapiro, G.I. and Gonzalez-Ondina, J.M., 2020. Seasonal Variability of Eddy Kinetic Energy in the Central Indian Ocean: POLYGON-67 Revised. *Physical Oceanography*, [e-journal] 27(6), pp. 573-589. doi:10.22449/1573-160X-2020-6-573-589

DOI: 10.22449/1573-160X-2020-6-573-589

© G. I. Shapiro, J. M. Gonzalez-Ondina, 2020

© Physical Oceanography, 2020

Introduction

Ocean observations carried out before the 1930s were separated by large intervals in space and time and therefore they supported the view of the low variability of physical fields in the water column except for the thin surface layer directly affected by the wind [1]. This point of view started to change in the late 1930s. In the Atlantic Ocean, some temperature and salinity fluctuations were observed at a transect between Nova Scotia and Bermuda which could have been an indication of the presence of an eddy [2]. In the Caspian Sea, a month-long time series at a fixed location demonstrated significant fluctuations of current velocity similar in nature to those occurring in small-scale turbulence. Statistical analysis revealed the presence of macro-turbulent eddies with periods from a few hours to a few days and a horizontal scale of a few kilometres [3, 4]. However, both methods – transects and time series at fixed stations – did not demonstrate a spatial

structure of the alleged eddies and therefore did not give any firm evidence of their existence. By the late 1940s the existence of Gulf Stream rings which were generated from cut-off Gulf Stream meanders were confirmed [5]. The traditional view at the time was that the eddies could only be formed in the vicinity of strong jet currents like the Gulf Stream, due to barotropic instability of the main current.

The breakthrough in our knowledge of ocean eddies came with the results of the POLYGON-67 experiment in the central Indian Ocean. It was the first direct and unambiguous observation that proved an earlier hypothesis by V. B. Shtockman, see [6] of the existence of mesoscale eddies in open ocean, not only next to strong jet-stream currents. Now it is well known that the currents in open ocean are almost everywhere dominated by mesoscale eddies also known as synoptic eddies [7]. POLYGON-67 experiment covered a rectangle bounded by 10–15°N and 63–66.5°E with a separation of the sampling sites by 0.5° both in the zonal and meridional direction. The experiment provided a nearly instantaneous snapshot of currents (January 21 – February 7, 1967). POLYGON-67 showed eddies of about 200 km in size, located closely to each other. The surface velocities calculated using a geostrophic method were about 0.1–0.2 m/s [8]. The second survey of the same area (March 20 – April 6) was carried out shortly after the first one and hence did not reveal seasonal variability of eddy parameters.

The purpose of this paper is to analyse the seasonal variability of mesoscale eddy activity in the area covered by POLYGON-67 using a modern and comprehensive data set over a period of 20 years from 1998 to 2017.

Materials and methods

The reliable high resolution data on currents as well as other oceanographic parameters can be obtained from the global ocean reanalysis data set produced by Mercator-Ocean and available from Copernicus Marine Environment Monitoring Service [<http://marine.copernicus.eu>]. For this study we use 1/12° resolution Global Ocean Physical Reanalysis product GLOBAL_REANALYSIS_PHY_001_030. The data set covers the period from 1993-01-01 to 2018-12-25, from which we selected a subset ranging from the 1st January 1998 to the 31st December 2017 using daily mean values of variables.

This product provides an eddy resolving (1/12°) global ocean simulation, covering the recent period during which altimeter data are available and constrained by assimilation of along-track Sea Level Anomaly, satellite Sea Surface Temperature and in situ temperature/salinity profiles. The results are interpolated from 1/12 degree native Arakawa C grid so that all variables are on the same regular grid points. For this study we are interested in the near-surface signature of eddy activity and hence we have selected the data at the depth level of 2.6 m to avoid artefacts at the very surface due to assimilation of satellite data. The study area coincided with POLYGON-67 and contained 61×43 grid points.

A typical horizontal scale of mid-ocean mesoscale eddies is about 100 km and a time scale is about 100 days, these mesoscale eddies have orbital speeds of the order of 0.1 m/s. Mesoscale ocean currents vary energetically in both time and space throughout the ocean [9]. As most of the kinetic energy is generally attributed to the mesoscale eddies while the majority of potential energy is contained in large scale ocean currents [10], the current study is focussed

exclusively on the kinetic energy variations associated with mesoscale currents as a first order effect.

There are different approaches that could be used in the definition of eddy kinetic energy, or *EKE*. One approach is to identify individual eddies as isolated coherent structures and calculate the energy and other characteristics only within such structures [11]. Another approach is to include in the definition of *EKE* the energy of all types of mesoscale currents such as the meandering and filamenting of intense current systems, semi-attached and cast-off ring currents, advective vortices extending throughout the entire water column, lens vortices, planetary waves, topographic waves, etc. All of these types of variable flows are commonly referred to by physical oceanographers by the generic term "eddies" and this study uses this more common approach [9].

An important issue is how to correctly separate the mesoscale fluctuations kinetic energy (hereafter *KE*) from the mean kinetic energy (*MKE*). The standard Reynolds-style approach is to decompose the components of velocity into mean (represented by overlines) and perturbation (represented by primes) parts [12,13]

$$u = \bar{u} + u', \quad (1)$$

$$v = \bar{v} + v', \quad (2)$$

where the mean values represent ensemble averaging

$$\bar{u} = \lim_{n \rightarrow \infty} \frac{1}{N} \sum_{k=0}^n u^{(k)}, \quad (3)$$

where $u^{(k)}$ is a member of a statistical ensemble, and a similar equation for v - component.

The ensemble averages satisfy the following conditions [13]:

$$\overline{\bar{u}} = \bar{u}, \quad \overline{u'} = 0, \quad \overline{uv} = \bar{u}\bar{v}, \quad \overline{u'v'} = \overline{v'u'} = 0. \quad (4)$$

Then the ensemble averaged full kinetic energy per unit mass (*FKE*) can be decomposed using equations (1) and (2) as follows

$$\overline{FKE} = \overline{\frac{1}{2}(u^2 + v^2)} = \overline{\frac{1}{2}(u^{\bar{2}} + 2\bar{u}u' + (u')^2 + v^{\bar{2}} + 2\bar{v}v' + (v')^2)} = \overline{MKE} + \overline{PKE} + \overline{CKE}, \quad (5)$$

where the mean kinetic energy *MKE*, perturbation kinetic energy *PKE* and cross-term kinetic energy *CKE* are defined as follows

$$MKE = \frac{1}{2}(\bar{u}^2 + \bar{v}^2), \quad PKE = \frac{1}{2}((u')^2 + (v')^2), \quad CKE = \bar{u}u' + \bar{v}v'. \quad (6)$$

By ensemble averaging equations (5) and using equations (3) and (4) one obtains

$$MKE = \overline{MKE}, \quad EKE = \overline{PKE} = \overline{\frac{1}{2}((u')^2 + (v')^2)}, \quad \overline{CKE} = 0. \quad (7)$$

From equation (7) it follows that the ensemble averaged full kinetic energy can be decomposed in only 2 terms, *MKE* and *EKE* as follows

$$\overline{FKE} = MKE + EKE. \quad (8)$$

Usually the ensemble averages are not available, and in practice, an ergodic hypothesis is applied that allows replacing the ensemble mean with a time average over the period when the process could be considered statistically in a steady state [12, Chapter 2 section 3]. In this case equation (8) is satisfied only approximately, and the time averaging of FKE gives

$$\langle FKE \rangle = MKE + EKE + \langle CKE \rangle, \quad (9)$$

where the angle brackets denote time averaging.

The time interval and method for averaging should be selected to minimise the cross-term $\langle CKE \rangle$ so that the last equation (7) is satisfied as closely as possible. This can be achieved if the averaging interval is large in comparison with the characteristic periods of the fluctuating quantities u' , v' , but small in comparison with the variability periods of slow varying quantities $\langle u \rangle$, $\langle v \rangle$ [13]. This means that the power spectrum of kinetic energy should ideally have a minimum separating fast and slow motions.

In order to find a suitable averaging interval, first the daily values of FKE at each grid cell inside the polygon are averaged over POLYGON-67 for each day of the 20-year long time series, see Fig. 1.

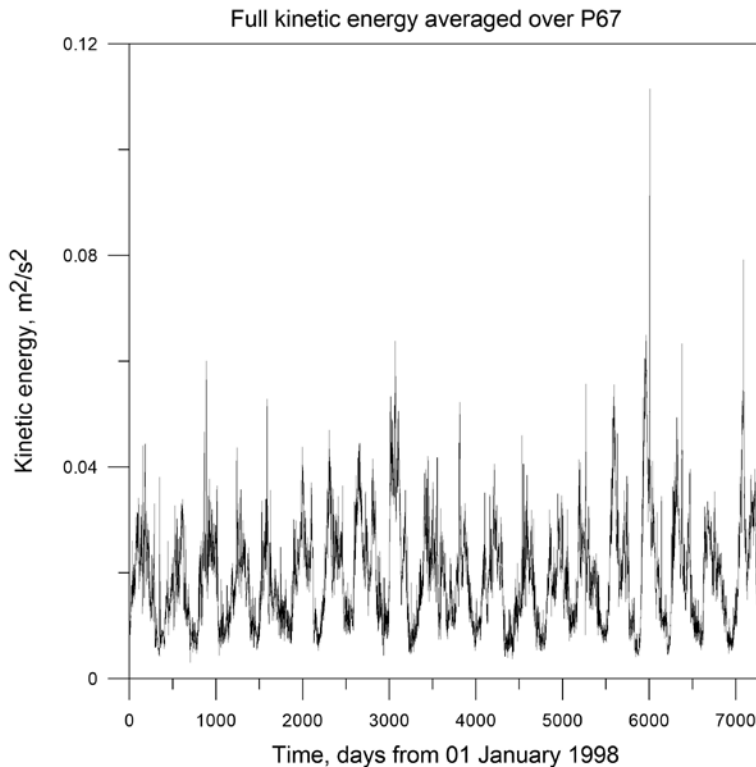


Fig. 1. Time series over 01/01/1998-31/12/2017 of full kinetic energy per unit mass at 2.6 m depth averaged over POLYGON-67 area

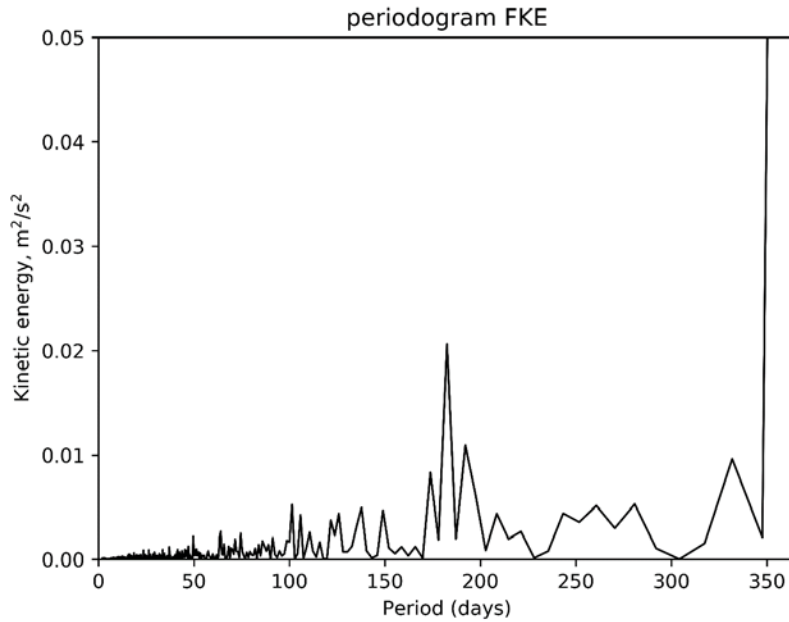


Fig. 2. Power spectral density of area averaged FKE using daily data from a 20-year long time series for the period 01/01/1998-31/12/2017

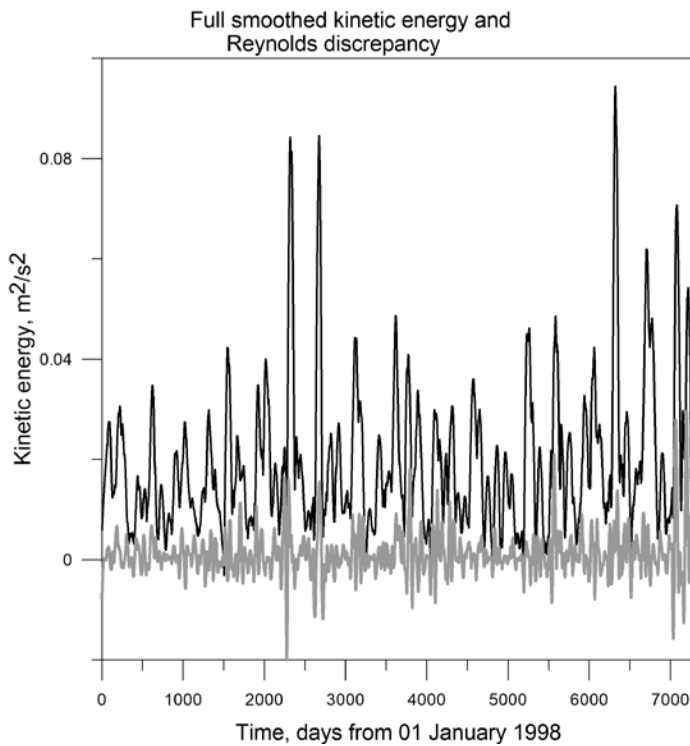


Fig. 3. Time series of time smoothed full kinetic energy $\langle FKE \rangle$ (black line) and the difference between $\langle FKE \rangle$ and the sum of $EKE + MKE$ (grey line) in the centre of POLYGON-67

The cut-off time period motion of $T = 103$ days used in this study is consistent with the results obtained in the equatorial Pacific Ocean [14] that defined mesoscale motion as having time scales of 6 to 66 days. The study of variability of zonal current velocity at 15 m depth in the equatorial Indian ocean have indicated a minimum in the density power spectrum at about $T = 80$ days, see Fig. 2, *b* in [15] which is closer to our results. Some researchers used the running average with a window of $T = 60$ days to separate mesoscale and slow processes in the equatorial Pacific Ocean [16], which is slightly shorter than the timescale used in this paper. On the other hand, a longer 300-day high-pass filter was used to assess contribution from the mesoscale eddy signals in the south-east Indian Ocean [17]. The adequacy of the selected time interval $T = 103$ days is assessed below.

The time series of velocities at each grid-point inside the study area were low-pass filtered using the Savitsky – Golay filter of the second order to obtain slow varying values $\langle u \rangle$, $\langle v \rangle$. The velocity perturbations are obtained by subtracting the slow varying quantities from full velocities. The slow varying values of $\langle FKE \rangle$, $EKE = \langle PKE \rangle$ are obtained from time series of FKE , PKE using the same filtering technique. Fig.3 shows the time series of $\langle FKE \rangle$ and the Reynolds discrepancy $\langle CKE \rangle$, i.e. the difference between $\langle FKE \rangle$ and $MKE + EKE$, to assess how well the Reynolds conditions given by equation (4) and equation (8) are satisfied, i.e. how well the slow varying component of full kinetic energy can be decomposed into MKE and EKE . In an ideal situation the Reynolds discrepancy should be zero. Fig. 3 shows that full kinetic energy is decomposed into MKE and EKE reasonably well with only a small interaction between slow and fast motion.

Results and discussion

In order to estimate the seasonal variability of KE , the 20 years long time series of area averaged EKE and MKE are cut into individual years and averaged over an ensemble of 20 members. The result is presented in Fig.4.

Seasonal variation of EKE reveals two peaks: in late April and beginning of October. The spring peak is approximately twice as high as the autumn one. A typical current velocity corresponding to the first and second peaks are $U_1 = 0.15$ m/s and $U_2 = 0.12$ m/s respectively. Mean kinetic energy has its main maximum (corresponding to $U_3 = 0.2$ m/s) in July when the EKE has a minimum. Mean kinetic energy is higher than eddy kinetic energy throughout the year. In December – January both EKE , and MKE have a minimum.

The higher level of EKE in summer than in winter is generally consistent with EKE variability observed in the southeast Indian Ocean where EKE displays a distinct seasonal cycle with a maximum in austral summer (November – January) and its minimum in austral winter (May – July) [17]. However, the double peak in the EKE , level shown in Fig. 4 is different from what was found to the south of the equator. The seasonal variability shown in Fig. 4 is also different from the tropical Pacific Ocean. Whilst in the tropical North Indian Ocean we see two strong maxima in the EKE , the tropical North Pacific has a strong minimum in April-May but stays high in the second half of year [14].

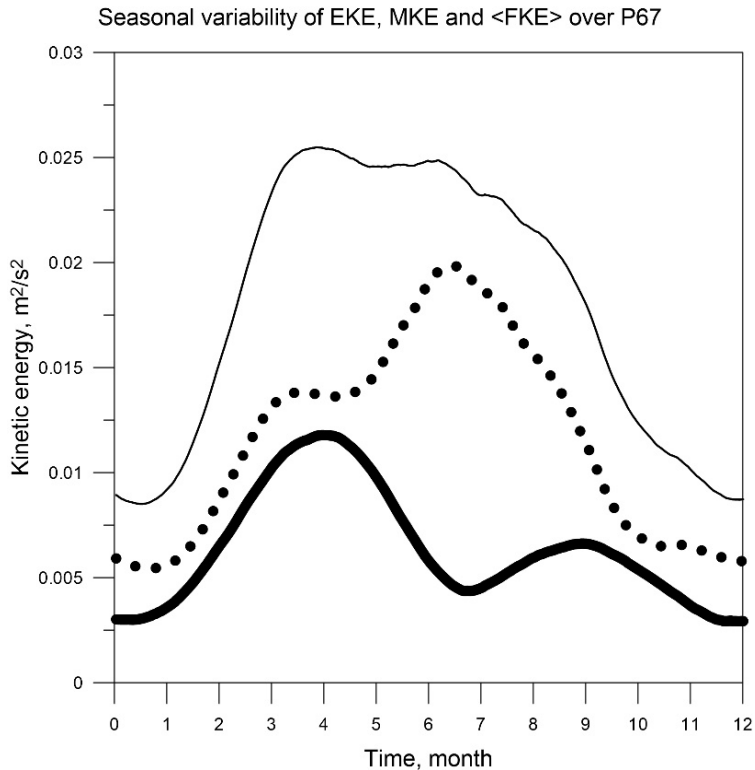


Fig. 4. Seasonal variability of eddy *EKE* (thick line), *MKE* (dotted line) and *EKE + MKE* (thin line) averaged over the POLYGON-67 area. All daily data are climatically averaged over 20 individual years from 1998 to 2017

Time smoothed full kinetic energy represented by *EKE + MKE* does not have pronounced extremes either in April or in October as the summer minimum in *EKE* is well compensated by the maximum in *MKE*. However the winter minimum is exhibited by both *EKE*, and *MKE* and, consequently, by *<FKE>* see Fig. 4.

The two main mechanisms of increasing *EKE* are baroclinic and barotropic instabilities of large-scale currents. Kinetic energy is converted from the mean flows to eddy flows by the barotropic instability of the horizontal circulation. The baroclinic process converts energy from the mean flow available potential energy to eddy energy, see [16, 18]. Baroclinic instability is related to the vertical shear of current velocity whilst the barotropic instability is generated by the horizontal shear of the velocity, which can be quantified by the enstrophy of the flow field. In order to assess a potential role of barotropic instability, the enstrophy $ENSTR = (rot_z \langle \mathbf{u} \rangle)^2$ of the slow varying flow field $\langle \mathbf{u} \rangle = (\langle u \rangle, \langle v \rangle)$ is calculated at each grid point as a function of time and then averaged over the polygon area. The seasonal variability is calculated by climatically averaging 20 individual years, see Fig. 5.

The two maxima in enstrophy occur at the same times as the maxima in *EKE*, namely in April and October, and the minima are also close: late July for *EKE* and mid-July for enstrophy. The Pearson correlation coefficient between 20 years long

time series of *EKE* and enstrophy is $R = 0.72 \pm 0.01$ at 95% confidence level. High correlation of *EKE* and enstrophy variability indicates in favour of the dominant role of barotropic instability in the formation, support and decay of mesoscale activity in the tropical Indian Ocean.

Our results show that the source of *EKE* in the central Indian Ocean is different from what was observed in the Pacific Ocean, where the energy sources for eddy kinetic energy within the Tropical Instability Waves area (10° S to 15° N) were demonstrated to be a mixture of barotropic and baroclinic instabilities in almost equal proportions [16, 19]. This difference is likely caused by different properties of the equatorial currents in the Pacific and Indian oceans. In the Pacific, there is a strong cold-water tongue along 4° N, the extension of the cold Humboldt Current [20]. The cold tongue is accompanied by a thermocline trough which results in strong meridional temperature and (available) potential energy gradients, which enhance the baroclinic energy conversion rate between eddy potential and eddy kinetic energies. In contrast, the Equatorial Current in the Indian Ocean is fed by warm water masses from the Pacific as maximum flow into the Indian Ocean occurs during the southeast monsoon from July to September [21].

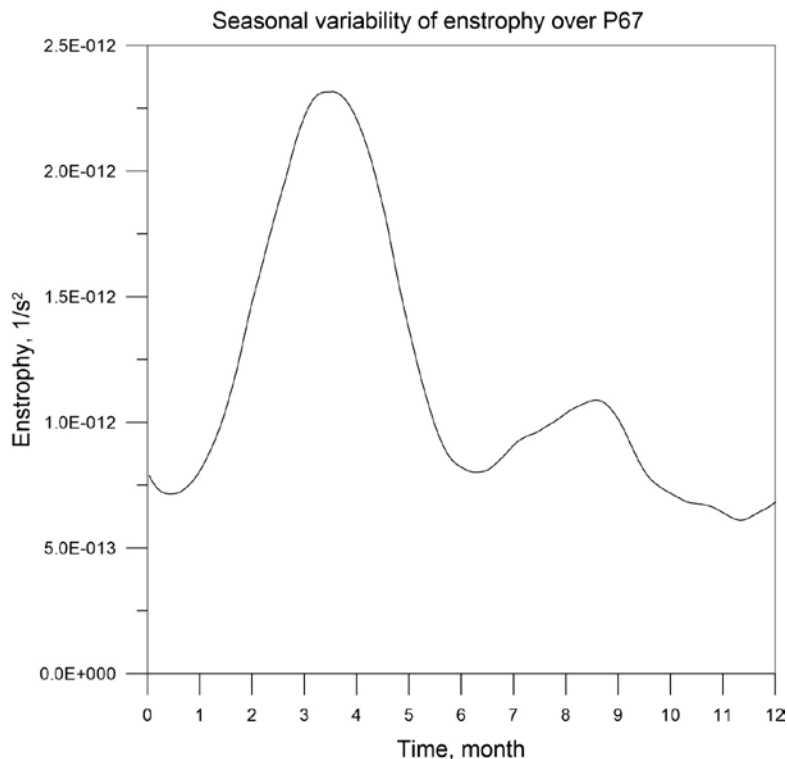


Fig. 5. Seasonal variability of enstrophy calculated from the slowly varying flow field over the POLYGON-67 area

It is known that weak eddies could be well described as quasi-geostrophic Rossby waves, while eddies with strong orbital velocities could be described as strongly non-linear waves or large ‘particles’ like the Mediterranean eddies.

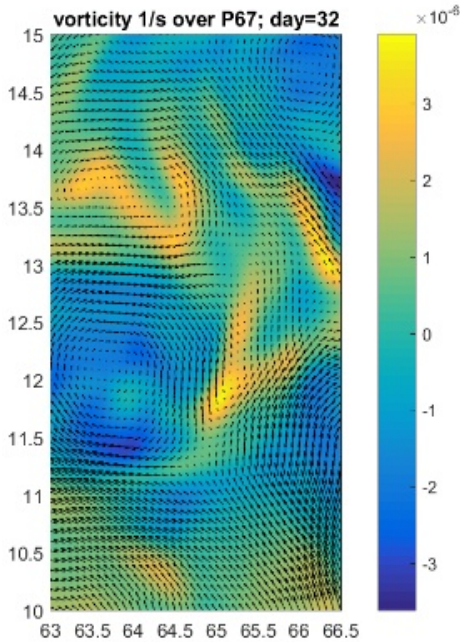


Fig. 6. A snapshot of current velocities (arrows) and vorticity (color) distributions within the POLYGON-67 area on 1st February 1998 showing eddies and other mesoscale structures

The Rossby waves become effective when the turn-around time of an eddy is greater than the planetary wave period. Then the energy can become wave-like and dispersed, and zonally dominant anisotropic flows are favoured [9, 22].

The structure of mesoscale activity within the polygon area is shown in Fig. 6 for approximately the same time of year (but a different year due to data availability) as the POLYGON-67 survey. A strong anticyclonic eddy of approximately 100 km in size is centred at 11.7° N, 63.5° E, and another half-anticyclone is seen to the east of it. There is a strong and large cyclonic eddy centred at 13.7° N, 64.2° E and a weaker anticyclonic eddy at 14.7° N, 66° E, whilst the rest of the area is filled with weaker meanders and filaments.

An approximate threshold size of an eddy to be considered as displaying Rossby wave properties is calculated using the scale analysis as follows. Let L be the diameter of an eddy and let U be its maximum orbital velocity. The phase speed of the Rossby wave is

$$C = \beta L^2 \text{ and hence the Rossby wave period is } T_R = \frac{L}{C} = \frac{1}{\beta L}, \text{ where } \beta = \frac{df}{dy}.$$

The period of eddy orbital rotation is $T_E = \pi L / U$, hence the threshold eddy diameter is $L_t = \sqrt{\frac{U}{\pi\beta}}$

The value of β in the middle of the polygon is $\beta = 2.3 \cdot 10^{-11} \text{ 1/ms}$. Hence $L_t = 0.6 \cdot 10^5 \text{ m} = 60 \text{ km}$. The mesoscale features larger than L_t should be affected by Rossby waves which travel zonally westward [7]. The eddies within the polygon area are typically of the order of 70–100 km, see Fig. 6, hence they should display a slightly stronger zonal translational velocities compared to the meridional ones. The prevailing transport of EKE based on the energy fluxes through the polygon boundaries is discussed further below.

A typical size of eddies can be estimated by computing the integral length scale from the transverse autocorrelation of the velocity components [23]. For this we have computed $R_{ii}(r)$ along a meridian for the zonal component of the velocity and along a parallel for the meridional component (see Fig. 7) using the expression:

$$R_{11}(r) = \frac{\langle \Delta u(0)\Delta u(r) \rangle}{\langle \Delta u(0)\Delta u(0) \rangle},$$

where $\Delta u = u - \langle u \rangle$ is the fluctuation of a demeaned velocity component when the spatial average over the POLYGON-67 area, denoted by symbol $\langle u \rangle$ is removed (similarly for R_{22} and v). The origin, at 12.5° N, 64.75° E, is located at the grid node closest to the centre of the POLYGON-67 area and r is the distance from the origin in a direction perpendicular to the velocity component. The integral length scales in the meridional ($i = 1$) and zonal ($i = 2$) directions can be calculated using the expression:

$$L_i = \int_0^d R_{ii}(r) dr,$$

where d can be ∞ , or the first zero crossing, or the first minimum of the autocorrelation function. In order to avoid problems created by noise at larger values of r and following the method used in [23], we have defined d as the first point where R_{ii} is equal to zero. Using this definition, we have computed the integral length scales along a meridian $L_1 = 52,1$ km and along a parallel $L_2 = 49,5$ km.

The integral length scales represent typical radii of an eddy and are consistent with our previous estimation of the eddy diameter (around 100 km) based on the analysis of daily maps of vorticity. Eddies exhibit some anisotropy being slightly more elongated in the meridional direction. The length scales shown above are consistent with those identified in the North Atlantic using the same method, where the lengths ranged from 42 to 68 km [23].

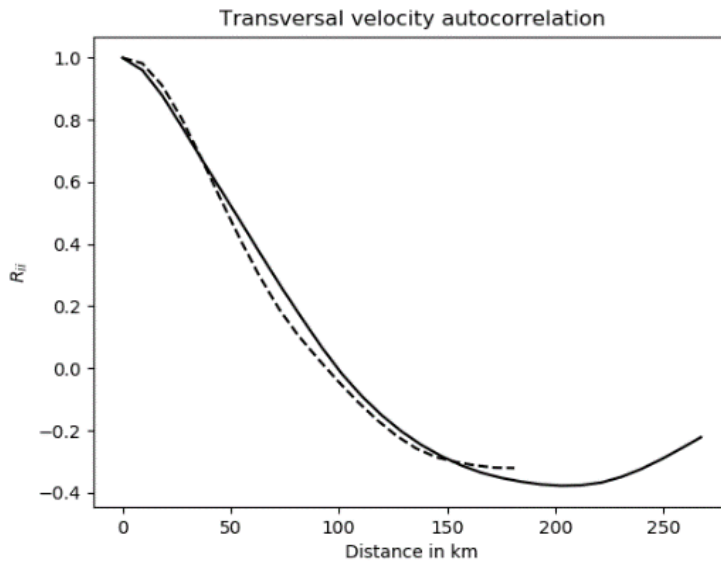


Fig. 7. Transverse autocorrelation function $R_{ii}(r)$ of the velocity components between the centre of the POLYGON-67 area and the variable point r . Solid line is for the zonal component and dashed line is for the meridional component

Fig. 8 shows the seasonal variability of transports of *EKE* across all polygon boundaries. The incoming zonal transport of *EKE* is relatively high at the western boundary during the summer season May to October, however it is small and directed outward at the eastern boundary. The outgoing *EKE* transport across the southern boundary (10° N) is significantly higher than the incoming transport across the northern boundary (15° N) during this period which indicates an action of a larger scale loop current through the polygon. Generally there is no significant zonal anisotropy in the transport of *EKE* which is predicted by Rossby wave theory. This fact indicates that the advection of *EKE* by large scale current has a more significant effect on advection of *EKE* than Rossby waves.

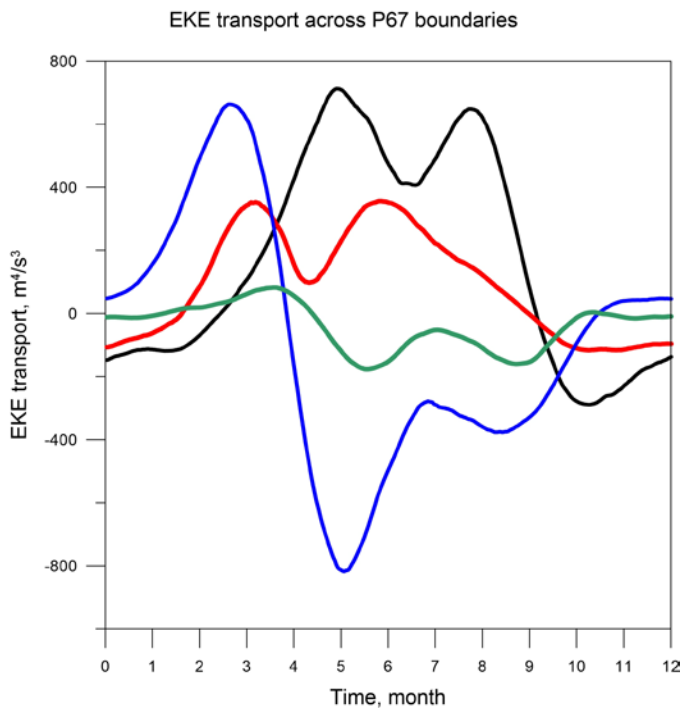


Fig. 8. Seasonal variability of *EKE* transports across 4 boundaries of the polygon. Transports through the west, east, south and north boundaries are shown by black, red, blue and green lines respectively

The structure of large-scale flow field and its seasonal variability is shown in Fig. 9. The 20-year long time series is first split into individual years, and then the velocity vectors are averaged for each of the 365 calendar days of the year, the leap year days are discarded. Then the vectors are averaged within each month. Typical monthly averaged current velocity is within the range of 0.1–0.2 m/s, which is the same order of magnitude as Rossby waves phase speed for $L = 100$ km of $C = 0.13$ m/s. This result is an additional confirmation that the lack of clear zonally dominated anisotropy in *EKE* fluxes is due to the combination of advection by larger-scale currents which has different direction in different seasons, and wave-like self-propagation which is always westward.

The direction of long-term averages of large-scale currents is consistent with monsoon circulation in the atmosphere, see Fig. 10: weaker easterly winds during November-January (5.4–7.4 m/s) and stronger westerly during May-September (3.4–12.6 m/s). The figures in brackets represent the maximum wind speeds over P67 area assessed using monthly long-term averages from NCEP/DOE AMIP-II Reanalysis (Reanalysis-2) Monthly Averages Data (*Reanalysis-2*) (URL: <https://psl.noaa.gov/>).

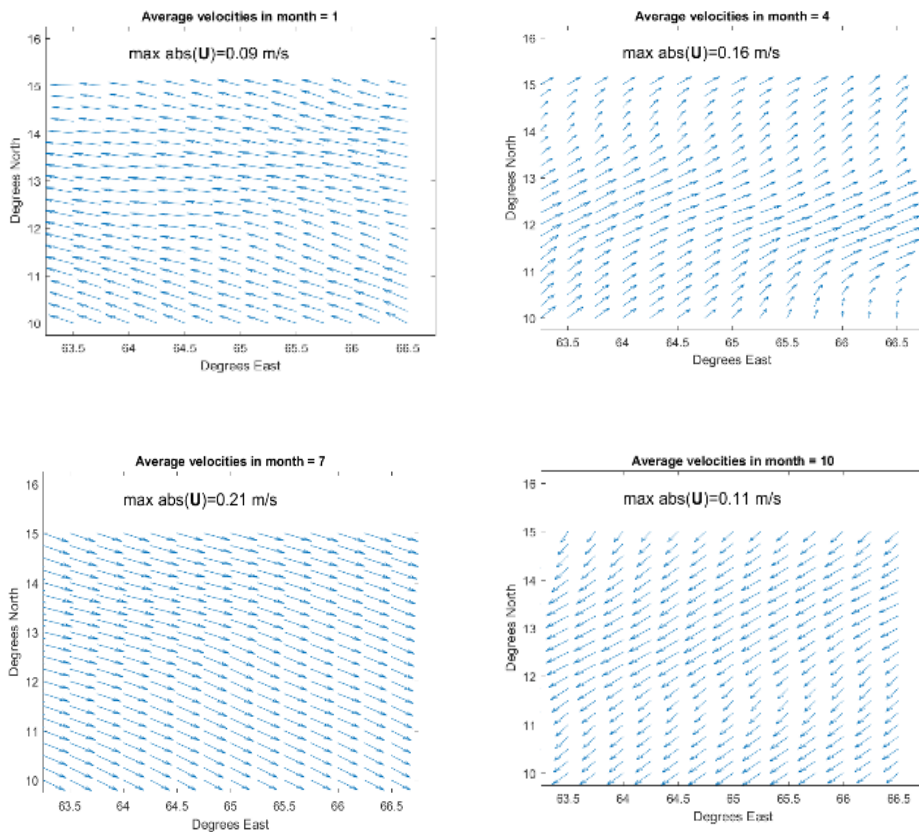


Fig. 9. Seasonal variability of large scale current through P67 shown by surface velocity fields for January, April, July and October. For clarity, only every third vector is shown

The evolution of *EKE* integrated within P67 can be represented by the equation

$$\frac{d}{dt} \iint_{P67} (EKE) dS = CONV + SOURCE, \quad (10)$$

where

$$CONV = - \oint_{\gamma P67} \mathbf{n} \cdot \mathbf{F} ds,$$

$\gamma P67$ is the rectangular boundary of POLIGON-67, \mathbf{n} is the outward normal unit vector, \mathbf{F} is the *EKE* flux per unit length of boundary and per unit depth defined as

$$\mathbf{F} = EKE \cdot \langle \mathbf{u} \rangle,$$

Here $\langle \mathbf{u} \rangle$ is the vector of time smoothed velocity. The terms in equation (10) have the following meaning: the term on the left hand side is the rate of change of *EKE*, integrated within P67, *CONV* is the convergences of *EKE* transports by ocean currents into the area of P67, *SOURCE* is the local area integrated source or sink of within P67 due to energy exchange between *EKE* and other types of energy.

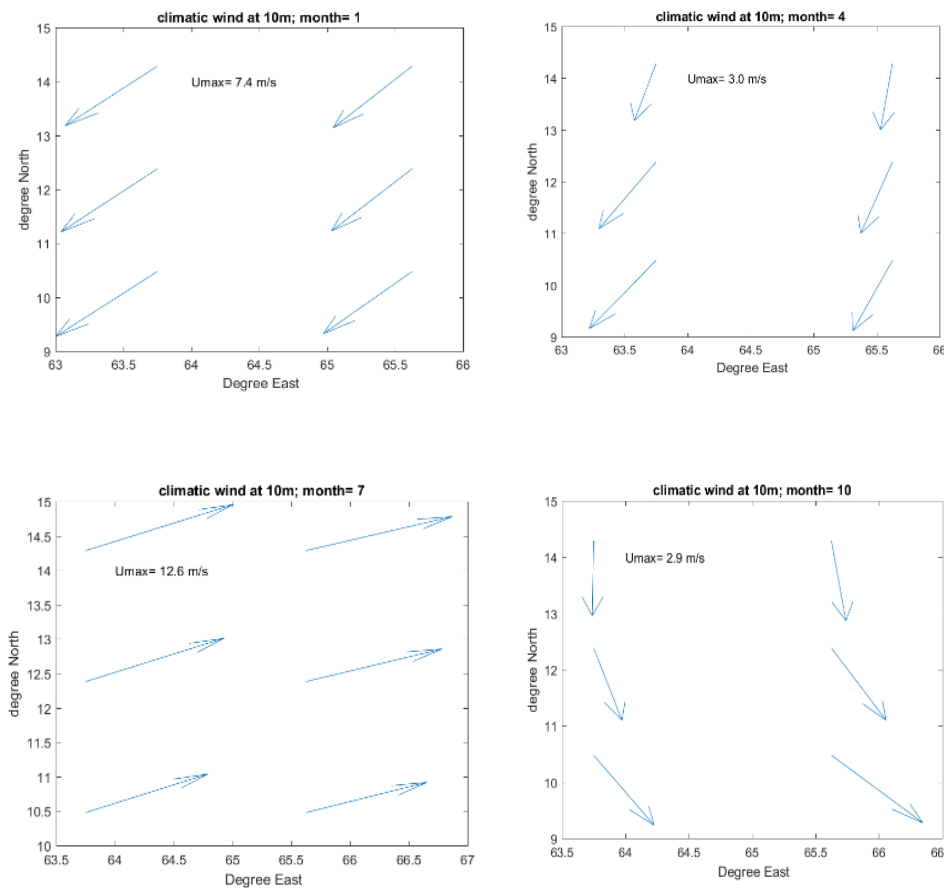


Fig. 10. Climatic wind over P67 area plotted using data from [<https://psl.noaa.gov/>]

Fig.11 shows seasonal variability of terms included in equation (10). From January to beginning of August changes in the *EKE* (blue line) are almost entirely due to advection of *EKE* (black line) from the neighbouring regions, local generation and decay of *EKE* is relatively small. From August to December the contribution of advected *EKE* and local sources/sinks are of the same order. Therefore, the spring maximum in *EKE* shown in Fig. 4 is almost entirely generated by the convergence of *EKE* transports from neighbouring regions, whereas the smaller autumn maximum is a result of joint action of local and non-local sources. In this context the high correlation of enstrophy and *EKE* during the spring maximum of *EKE* gives an indication that conversion of kinetic energy of large scale currents into mesoscale happens both inside and outside of P67 area.

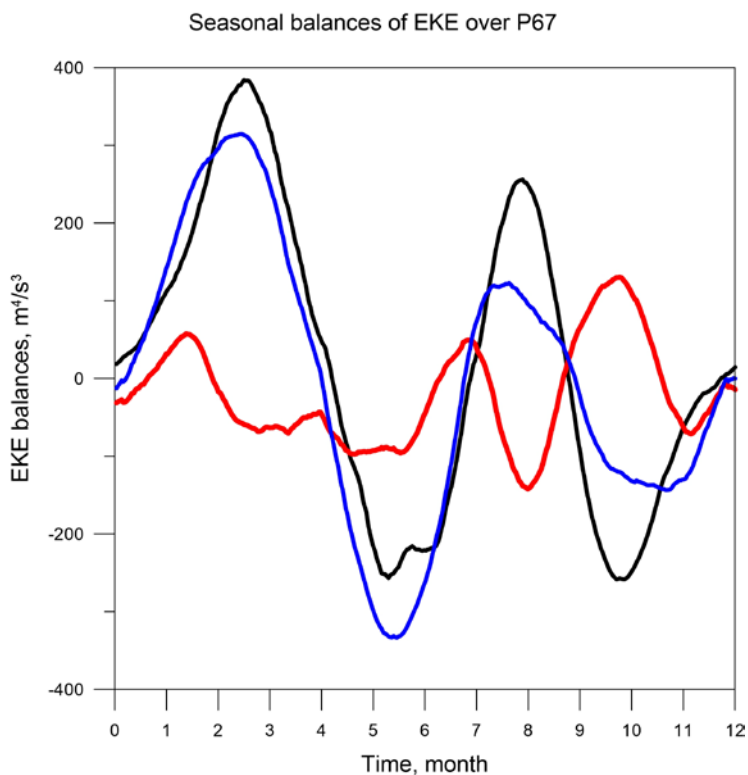


Fig. 11. Components of *EKE* conservation equation. Convergence of *EKE* transports into the P67 area (*CONV*, black); Local sources/sinks of *EKE* integrated over P67 (*SOURCE*, red); the rate of change of *EKE* integrated within P67 (blue). All values per unit depth of water at a depth level 2.6 m

Conclusion

The 20-year long eddy resolving reanalysis of velocity fields in the Indian Ocean allows the study of seasonal variability, dynamics and generation mechanisms of eddy kinetic energy (*EKE*) in the tropical Indian Ocean, including the area covered by the original survey of POLYGON-67 (P67) experiment. In

contrast to some other areas of the World Ocean, the *EKE* seasonality shows two maxima – the large one in April and the secondary one in October. The main mechanism of *EKE* generation is the barotropic instability which is evidenced by high correlation of enstrophy of large-scale currents, representing the strength of horizontal shear, and *EKE*. It is found that the main contributor to the *EKE* variability within P67 is advection of *EKE* across the P67 boundaries during January – October, while the local generation has a comparable magnitude during August – December. The direction and strength of surface currents is consistent with the monsoon wind pattern in the area.

REFERENCES

1. Stockman, V.B., Koshlyakov, M.N., Ozmidov, R.V., Fomin, L.M. and Yampolsky, A.D., 1969. Long-Term Measurements of the Physical Field Variability on Oceanic Polygons, as a New Stage in the Ocean Research. *Doklady AN SSSR*, 186(5), pp. 1070-1073. Available at: http://www.mathnet.ru/php/archive.phtml?wshow=paper&jrnid=dan&paperid=34699&option_lang=eng [Accessed: 11.12.2020] (in Russian).
2. Iselin, C.O'D., 1936. *A Study of the Circulation of the Western North Atlantic*. Papers in Physical Oceanography and Meteorology, 4(4). Cambridge, Massachusetts, 110 p. Available at: <https://core.ac.uk/download/pdf/4165652.pdf> [Accessed: 11.12.2020].
3. Shtokman, V.B. and Ivanovskiy, I.I., 1937. Results of Structural Study of Currents near the Western Coast of the Middle Caspian. *Meteorologiya i Gidrologiya*, (4). pp. 154-160 (in Russian).
4. Shtokman, V.B., 1941. On the Pulsations of the Horizontal Components of Velocity of the Ocean Currents Caused by Large-Scale Turbulence. *Doklady AN SSSR. Seriya Geograficheskaya i Geofizicheskaya*, (4-5), pp. 475-486 (in Russian).
5. Fuglister, F.C. and Worthington, L.V., 1947. *Hydrography of the Western Atlantic; Meanders and Velocities of the Gulf Stream*. Woods Hole Oceanogr. Inst. Tech. Rep. No. WHOI 47-9. Woods Hole, Mass.: Woods Hole Oceanographic Institution.
6. Koshlyakov, M.N., Morozov, E.G. and Neiman, V.G., 2016. Historical Findings of the Russian Physical Oceanographers in the Indian Ocean. *Geoscience Letters*, 3, 19. doi:10.1186/s40562-016-0051-6
7. Kamenkovich, V.M., Koshlyakov, M.N. and Monin, A.S., 1986. *Synoptic Eddies in the Ocean*. Dordrecht: Springer, 444 p. <https://doi.org/10.1007/978-94-009-4502-9>
8. Koshlyakov, M.N., Galerkin, L.I. and Tru'ong Dinh Hiê'n, 1970. On Mesostructure of Geostrophic Currents in the Open Ocean. *Okeanologiya*, 10(5), pp. 805-814.
9. Robinson, A.R., ed., 1983. *Eddies in Marine Science*. Berlin, Heidelberg: Springer, 612 p. doi:10.1007/978-3-642-69003-7

10. Ferrari, R. and Wunsch, C., 2009. Ocean Circulation Kinetic Energy: Reservoirs, Sources, and Sinks. *Annual Review of Fluid Mechanics*, 41, pp. 253-282. <https://doi.org/10.1146/annurev.fluid.40.111406.102139>
11. Xu, C., Shang, X.-D. and Huang, R.X., 2014. Horizontal Eddy Energy Flux in the World Oceans Diagnosed from Altimetry Data. *Scientific Reports*, 4, 5316. <https://doi.org/10.1038/srep05316>
12. Monin, A.S. and Yaglom, A.M., 1971. *Statistical Fluid Mechanics, Vol. 1. Mechanics of Turbulence*. London: The MIT Press, 769 p.
13. Kochin, N.E., Kibel', I.A. and Roze, N.V., 1963. *Theoretical Hydromechanics*. London: John Wiley & Sons, Ltd., 592 p.
14. Wang, M., Du, Y., Qiu, B., Xie, S.-P. and Feng, M., 2019. Dynamics on Seasonal Variability of EKE Associated with TIWs in the Eastern Equatorial Pacific Ocean. *Journal of Physical Oceanography*, 49(6), pp. 1503-1519. doi:10.1175/JPO-D-18-0163.1
15. Nagura, M. and McPhaden, M.J., 2012. The Dynamics of Wind-Driven Intraseasonal Variability in the Equatorial Indian Ocean. *Journal of Geophysical Research: Oceans*, 117(C2), C02001. doi:10.1029/2011JC007405
16. Wang, M., Du, Y., Qiu, B., Cheng, X., Luo, Y., Chen, X. and Feng, M., 2017. Mechanism of Seasonal Eddy Kinetic Energy Variability in the Eastern Equatorial Pacific Ocean. *Journal of Geophysical Research: Oceans*, 122(4), pp. 3240-3252. <https://doi.org/10.1002/2017JC012711>
17. Jia, F., Wu, L. and Qiu, B., 2011. Seasonal Modulation of Eddy Kinetic Energy and Its Formation Mechanism in the Southeast Indian Ocean. *Journal of Physical Oceanography*, 41(4), pp. 657-665. <https://doi.org/10.1175/2010JPO4436.1>
18. Cox, M.D., 1980. Generation and Propagation of 30-Day Waves in a Numerical Model of the Pacific. *Journal of Physical Oceanography*, 10(8), pp. 1168-1186. [https://doi.org/10.1175/1520-0485\(1980\)010<1168:GAPODW>2.0.CO;2](https://doi.org/10.1175/1520-0485(1980)010<1168:GAPODW>2.0.CO;2)
19. Luther, D.S. and Johnson, E.S., 1990. Eddy Energetics in the Upper Equatorial Pacific during the Hawaii-to-Tahiti Shuttle Experiment. *Journal of Physical Oceanography*, 20(7), pp. 913-944. [https://doi.org/10.1175/1520-0485\(1990\)020<0913:EEITUE>2.0.CO;2](https://doi.org/10.1175/1520-0485(1990)020<0913:EEITUE>2.0.CO;2)
20. Chavez, F.P., Bertrand, A., Guevara-Carrasco, R., Soler, P. and Csirke, J., 2008. The Northern Humboldt Current System: Brief History, Present Status and a View towards the Future. *Progress in Oceanography*, 79(2-4), pp. 95-105. <https://doi.org/10.1016/j.pocean.2008.10.012>
21. Meyers, G., Bailey, R.J. and Worby, A.P., 1995. Geostrophic Transport of Indonesian Throughflow. *Deep Sea Research Part I: Oceanographic Research Papers*, 42(7), pp. 1163-1174. [https://doi.org/10.1016/0967-0637\(95\)00037-7](https://doi.org/10.1016/0967-0637(95)00037-7)
22. Bower, A.S., Armi, L. and Ambar, I., 1997. Lagrangian Observations of Meddy Formation during a Mediterranean Undercurrent Seeding Experiment. *Journal of*

Physical Oceanography, 27(12), pp. 2545-2575. [https://doi.org/10.1175/1520-0485\(1997\)027<2545:LOOMFD>2.0.CO;2](https://doi.org/10.1175/1520-0485(1997)027<2545:LOOMFD>2.0.CO;2)

23. Le Traon, P.Y., Rouquet, M.C. and Boissier, C., 1990. Spatial Scales of Mesoscale Variability in the North Atlantic as Deduced from Geosat Data. *Journal of Geophysical Research: Oceans*, 95(C11), pp. 20267-20285. <https://doi.org/10.1029/JC095iC11p20267>

About the authors:

Georgy I. Shapiro, Head of the Plymouth Ocean Forecasting Centre, Professor at the University of Plymouth (University of Plymouth, Drake Circus, Plymouth, PL4 8AA, UK), Dr. Sci. (Phys.-Math.), **ORCID ID: 0000-0002-6740-8639**, gshapiro@plymouth.ac.uk

José María Gonzalez-Ondina, Senior Research Associate, Plymouth Ocean Forecasting Center, Ph. D. (University of Plymouth, Drake Circus, Plymouth, PL4 8AA, UK), **ORCID ID: 0000-0003-3918-2182**

Contribution of the co-authors:

Georgy I. Shapiro – conceptualization, methodology, software, investigation, writing up

José María Gonzalez-Ondina – software, investigation, validation, analysis, data curation

All the authors have read and approved the final manuscript.

The authors declare that they have no conflict of interest.